Screen-printed electrodes decorated with low content Pt–Ni microstructures for sensitive detection of Zn(II), ascorbic acid and paracetamol in pharmaceutical products and human blood samples

Fatima Zahra Makhlouf [a], Mohamed Lyamine Chelaghmia [a,*], Rafiaa Kihal [a,b], Craig E. Banks [c], Hassina Fisli [d], Mouna Nacef [a], Abed Mohamed Affoune [a], Maxime Pontié [e]

[a] *Laboratory of Industrial Analysis and Materials Engineering, University May 8, 1945 Guelma, P.O.B. 401, Guelma 24000, Algeria*
[b] *Abbes Laghrour University Khenchela, P.O.B 1252 Road of Batna, Khenchela 40004, Algeria*
[c] *Faculty of Science and Engineering, Manchester Metropolitan University, Chester Street, Manchester M1 5GD, UK*
[d] *Laboratory of Applied Chemistry, University May 8, 1945 Guelma, P.O.B. 401, Guelma 24000, Algeria*
[e] *Analysis and Process Group, University of Angers, Faculty of Sciences, 2 Bd. Lavoisier, 49045 Angers cedex 01, France*

In this study, we report for the first time, a method for simultaneous detection of paracetamol (PA) and its toxic impurities, 4-aminophenol (4-AP), as well as commonly co-formulated drugs, ascorbic acid and zinc (AA and Zn (II)), using screen-printed electrodes (SPEs) as a sensing platform. To improve the electrochemical performance of the SPEs, these are decorated with platinum and nickel microstructures (Pt–Ni), using a simple electrode- position technique. The structures and morphologies of the synthesized Pt–Ni/SPE electrode were confirmed by FE–SEM, TEM, EDX, XRD and AFM measurements. Furthermore, electrochemical characterization of the as-prepared sensor was investigated using cyclic voltammetry and electrochemical impedance spectroscopy methods. Under optimum conditions, the content of 4-AP, PA, AA and Zn(II) was quantified using cyclic vol- tammetry, differential pulse voltammetry and square-wave voltammetry techniques. The designed sensor exploits a dual effect, leveraging the efficiency of Pt for Zn(II) detection and Pt–Ni for the detection of 4-AP, AA, and PA. On one hand the as-prepared Pt–Ni/SPE sensor exhibits a linear response towards 4-AP and PA, ranging from 0.5 to 200 μM for both, with detection limits of 0.33 μM and 0.23 μM (S/N = 3) for 4-AP and PA, respectively. On the other hand, it demonstrates a linear response towards PA, AA, and Zn(II), ranging from 0.01 to 0.8 μM for Zn(II), 10 to 1800 μM for AA, and 0.5 to 200 μM for PA, with detection limits of 0.004 μM, 9.0 μM, and 0.15 μM for Zn(II), AA, and PA, respectively. Crucially, the as-fabricated sensor, with its remarkable reproducibility, recovery, long-term stability, and anti-interference capabilities, effectively quantified 4-AP, PA, Zn(II) and AA in both pharmaceutical formulations and human plasma samples.

1. Introduction

Paracetamol (PA), commonly known as acetaminophen or N-acetyl-p-aminophenol [1], is a widely used analgesic and antipyretic medication renowned for its effectiveness in reducing fever [2] and relieving mild to moderate pain, including migraine, backache, neuralgia, arthritis, cancer pain and postoperative pain [3,4]. Moreover, PA can be used as a good alternative for patients with aspirin allergy [5,6]. At nominal therapeutic doses, PA stands out as one of the relatively safest over the counter (OTC) drugs. It is extensively used by a diverse kind of patients, covering children, adults, and expectant mothers, both within and outside hospital settings [7]. Nevertheless, overuse of PA may result in the accumulation of toxic metabolites, leading to serious complications such as hepatotoxicity, nephrotoxicity, skin rashes, inflammation of the pancreas, liver and kidney damage with reported cases of fatal outcomes annually in the UK [8–10]. 4-Aminophenol (4-AP) is the main hydrolytic degradation product of paracetamol. As a synthetic intermediate or decomposition product of PA in pharmaceutical preparations, 4-AP possesses significant nephrotoxicity and teratogenic effect to the human body [11,12]. Therefore, the maximum allowable content of 4-AP in PA pharmaceutical formulations is limited to 50 ppm (0.005 %, w/w) by the European, United States and Chinese pharmacopeias [13].

Ascorbic Acid (AA) or vitamin C is an essential micronutrient for humans that occurs abundantly in many fresh fruits, beverages and

* Corresponding author.

vegetables and it is an antioxidant, helpful for both preventing and treating certain diseases such like infertility, common cold, cancer, cardiovascular disease, acquired immune deficiency syndrome (AIDS), healing of wounds, and oxidative stress (fatigue) [14–16]. The recommended daily intake of AA in biological fluids ranges from 70 mg to 90 mg, and its concentration has been proposed as an indicator of health [17]. Lacking of AA often causes gum bleeding, deterioration of collagen, scurvy, and anemia [18,19]. Since the human body cannot produce vitamin C internally, individuals consume medicinal supplements and canned fruit juices as alternative sources of AA. However, excessive intake of AA from various sources is often associated with abdominal cramps, diarrhea, and early signs of scurvy [20].

Likewise, Zinc (Zn(II)) is also recognized as a vital nutrient for human beings, playing a crucial role in regulating various biological processes, including gene transcription, DNA synthesis, cellular metabolism, immune function, and serving as catalysts for over 200 enzymes [21,22]. This cation is not naturally produced in the body and is obtained through dietary sources or by taking a nutritional supplement [23]. Conversely, abnormal levels of Zn(II) can be toxic, leading to consequences such as Alzheimer's disease, epilepsy, nausea, diarrhea, kidney organ damage, and even death in severe cases [24–26].

In the current trend, self-medication is prevalent, with people relying on over the counter aforementioned drugs and nutrient tablets for immune support or disease treatment, as seen during the Covid-19 pandemic. Individuals often self-prescribe drugs, spurred by studies suggesting their effectiveness against the virus. This leads to the unregulated use of combination medications to enhance symptom relief, even though some have been proven ineffective [27]. Ignoring recommended dosages, people risk overdose symptoms like hypotension and flaccidity, potentially resulting in death. To address this, there is a crucial need for sensitive analytical methods for the early detection of definite target analytes such as fluorescence [28], direct titration [14], HPLC [29], capillary electrophoresis [30], and so on. Although the determination of PA, 4-AP, AA and Zn(II) using these methods typically have shown high sensitivities, they suffer from several disadvantages, including the need for skilled operators, expensive instruments, time-consuming and complex sample preparations, which make them impractical for routine analysis of target analytes [12]. Due to the electroactive nature of PA, 4-AP, AA and Zn(II) compounds, electrochemical based voltammetric methods combined with electrochemical sensors offer a better alternative for their quantification. Their high selectivity, low cost, ease of operation and on-site monitoring capabilities render them an invaluable tool in the field of clinical diagnostics, as well as in biological and environmental analysis [2,31]. Additionally, to improve the sensitivity and selectivity of electrochemical sensors, researchers have used various active materials to modify the working electrode surface. These modified electrodes exhibit enhanced catalytic activity, a larger surface area, a lower detection limit, and improved selectivity in the electrochemical detection of diverse biological and pharmaceutical species [32–35].

In recent years, screen-printed electrodes (SPEs) have drawn many merits in several areas, particularly in their application in electroanalysis [36] and offer advantages of disposability, fast response, low cost, easy portability, flexibility in design and overcome the need for additional pre-treatment steps, such as mechanical activation (polishing), commonly associated with conventional solid carbon electrodes [37,38]. These disposable SPEs generally consist of a three-electrode configuration, a working electrode on which electrochemical reactions occur, counter and pseudo-reference electrodes. The working electrode can be produced by screen-printing various kinds of inks on different substrates (i.e., ceramic, plastic, or printed circuits) [39]. A major benefit of screen-printing technology is that it offers process automation, a wide selection of electrodes and the manufacture of highly reproduc- ible and economical single-shot sensors. For these reasons, SPEs modi- fication with variety of nanomaterials [37,40,41], especially oversized noble metals chosen for their large surface area, reduction of over potential and exceptional electro-catalytic ability [24,42–44], via electrochemical deposition could serve as an interesting technique for generating electrochemical sensors that are specific and selective towards analytes of interest.

One of the noble metal nanoparticles that is often used as an electrode modifier is platinum nanoparticles (PtNPs), because of their superior electro-catalytic as well as electronic properties [45–47]. However, Pt has long struggled with its surface being rapidly and easily poisoned by strongly adsorbed intermediates [48]. This drawback can be effectively addressed by creating bimetallic materials, where the incorporation of Pt with another transition metal enhances both the synergistic and electronic properties. In the synergistic process, the secondary metal plays a pivotal role in facilitating oxidative removal of the blocking residues at the Pt active sites [49,50]. It is well established that nickel (Ni) is one of the widely researched transition metal, given its attractive features, such as reliable stability, cost-effectiveness, abundant availability, and environmental friendliness [51,52]. Hence, the bimetal (Pt–Ni) systems have been extensively reported in many fields. Aysun et al. made a novel enzyme-free biosensor by modifying the surface of a glassy carbon electrode with activated carbon-supported Pt–Ni nanocomposites (PtNi@AC) for glucose determination. The prepared electrode showed excellent sensitivity and stability [53]. A fluorine doped tin oxide coated glass modified with mixed Pt–Ni hydroxide nanoparticles fabricated by Nath´alia et al. was shown to be effective as BIA amperometric sensor for determination of hydralazine in pharmaceuticals [54]. Liang and colleagues prepared a new sensor based on Pt–$Ni(OH)_2$ nanoflakes via one-step galvanic replacement reaction, for ammonia–nitrogen detection in drinking water. The constructed sensor exhibited a high sensitivity of 1.79 $\mu A\ \mu M^{-1}cm^{-2}$ [55]. Chelaghmia et al. also reported an ethanol electro-oxidation in alkaline medium using activated graphite supported Pt–Ni prepared by electrodeposition method [56].

In this work, we introduce for the first time, screen-printed electrodes decorated with Pt–Ni bimetallic particles via a facile and effective electrodeposition technique for the simultaneous detection of PA and its toxic impurity, 4-AP, in PBS solution, as well as for the simultaneous determination of Zn(II), AA, and PA in ABS solution. The analytical parameters (selectivity, linearity, detection limit, reproducibility) of the electrochemical sensor for PA, 4-AP, AA, and Zn(II) were investigated using CV, DPV, and SWV techniques.

Finally, the practical performance of the sensing electrode was evaluated by the simultaneous detection of AA and PA, as well as Zn(II) and AA, for precise quality control of pharmaceutical products, and by the simultaneous triple detection of Zn(II), AA, and PA in a single analytical run in human blood samples without significant interferences.

2. Experimental section

2.1. Reagents

All chemicals were of analytical grade and used without any further purification and doubly distilled water with a resistivity of 18 MΩ cm was used to prepare all aqueous solutions. Nickel sulfate hexahydrate ($NiSO_4\ 6H_2O$), sodium sulfate (Na_2SO_4), chloroplatinic acid ($H_2PtCl_6\ 6H_2O$), paracetamol (PA), 4-aminophenol (4-AP), ascorbic acid (AA), caffeine (Caf), glucose (Glu), fructose (Fru), galactose (Gal), citric acid (Cit) and potassium hexacyano ferro/ferrate ($K_3Fe(CN)_6$ / $K_4Fe(CN)_6$), were procured from Sigma-Aldrich, Germany. Stock solution of Zn(II) (1000 mg L^{-1}) was supplied from PerkinElmer-Pure, USA. The phosphate buffer solution (PBS, 0.1 M) with a pH of 7.4 was gained by mixing 0.1 M NaH_2PO_4 and Na_2HPO_4, whereas the acetate buffer solution (ABS, 0.1 M) with a pH of 4.7 was a mixture of 0.1 M CH_3COONa and CH_3COOH. The commercial pharmaceutical tablets (Doliprane tablet, Efferalgan Vitamin C tablet and Vitamin C with Zinc complementary dietary supplement) were purchased from a local pharmacy.

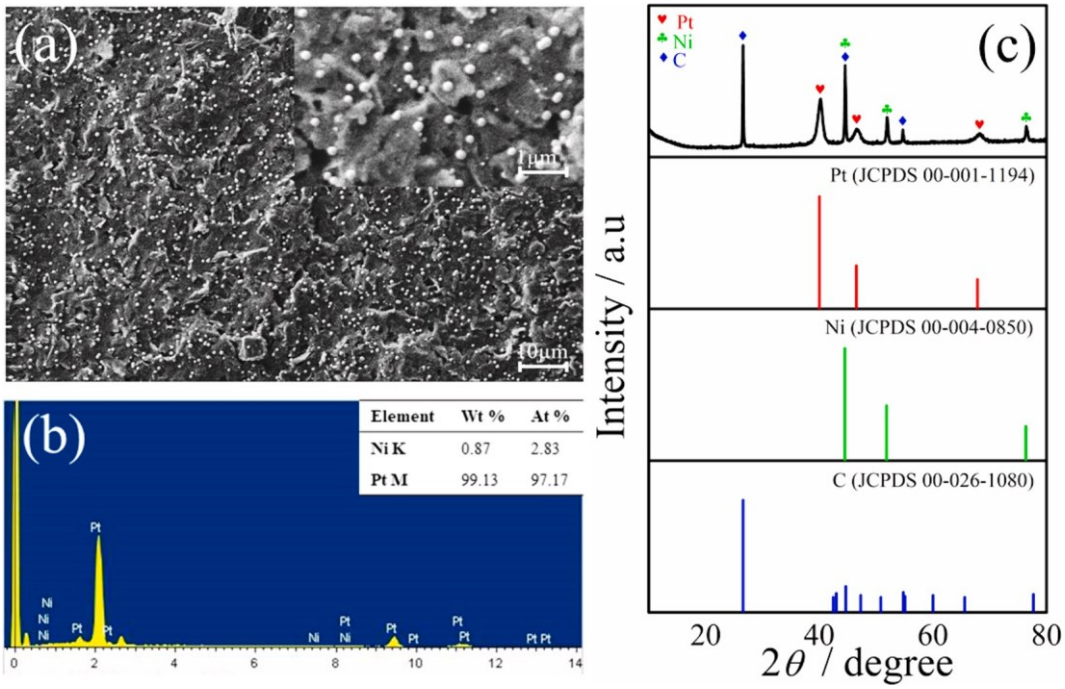

Fig. 1. FE–SEM images (a), EDX spectrum (b), and XRD pattern (c) of Pt–Ni/SPE electrode.

2.2. Preparation of the modified screen-printed electrodes (SPEs)

The screen-printed electrodes are fabricated using stencil designs and a micro DEK 1760RS screen-printing machine (DEK, Weymouth, UK). For the fabrication, initially, a carbon-graphite ink formulation extensively used in previous works [57–60] was screen-printed onto a flexible film made of polyester (Autostat, 250 μm thickness). The curing process for this layer involved placing it in a fan oven at 60 °C for a duration of 30 min. Following this, an Ag/AgCl reference electrode was created by screen-printing Ag/AgCl paste (Gwent Electronic Materials Ltd., UK) onto the plastic substrate. The connection was finalized and the 3.1 mm diameter graphite working electrode was defined by printing a dielectric paste ink (Gwent Electronic Materials Ltd., UK). After undergoing a final curing process at 60 °C for 30 min, the screen-printed graphite electrodes are now prepared for use.

The SPEs' working electrodes were modified with Pt–Ni nanostructures via electrodeposition technique using linear sweep voltammetry only in the cathodic direction, ranging from 0 V to –0.95 V, repeated 5 times in an aqueous solution. The innovative utilization of the electrodeposition technique mentioned in this study not only effectively reduced concentration polarization but also significantly elevated grain refinement. The platinum and nickel (Pt–Ni) were simultaneously electrodeposited in a 1.0 M H_2SO_4 solution containing a mixture of 8.0 mM H_2PtCl_6 and 128 mM $NiSO_4$. Afterwards, the modified electrode was washed thoroughly with distilled water, and left to dry naturally at room temperature. Prior to use, the modified Pt–Ni/SPE electrode was subjected to at least fifty CV cycles in the potential window of –0.8 to 1.0 V in 0.1 M PBS solution (pH 7.4) at 50 mV s^{-1} until a stable peak response is reached (Fig. S1). For comparison, SPE modified with PtNPs was also elaborated following an identical procedure, using as a precursor only 8.0 mM H_2PtCl_6.

2.3. Instruments and electrochemical experiments

The morphological features and elemental composition of SPE-modified electrodes were investigated via field emission scanning electron microscope (FE–SEM) coupled with energy dispersive X–ray spectroscopy (EDX) (JEOL, 6301F, Japan). The transmission electron microscope (TEM) image was obtained at JEOL, JEM-1400 TEM (Japan). The crystalline structure of the Pt–Ni/SPE modified electrodes was studied by X–ray diffractometry (XRD) on a Bruker D8 Discover spectrometer with Cu-Kα radiation (λ = 1.5418). The atomic force microscopy (AFM) images were obtained using a Nanoscope III from Bruker, Germany. The voltammetric measurements were conducted using a potentiostat (Princeton Applied Research, AMETEK, USA). All electrochemical measurements were carried out using SPEs with a three-electrode configuration, a working electrode consisting of either graphite or graphite decorated with Pt, or a combination of Pt and Ni microstructures (Φ = 3.1 mm), a graphite auxiliary electrode and an Ag/AgCl reference electrode. All potentials were expressed with respect to the screen-printed Ag/AgCl electrode. CV, DPV and SWV techniques were used to evaluate the electro-catalytic performance of the modified SPEs. CV was recorded in the potential range from –0.8 to 1.0 V in 0.1 M PBS solution (pH 7.4) at a scan rate of 50 mVs^{-1} for 4-AP and PA detection. For DPV and SWV measurements, various concentrations of the target analytes were deposited onto the working electrode surface by applying a potential of –0.6 V for 20 s, facilitating the simultaneous detection of 4-AP and PA, as well as the simultaneous detection of AA and PA, accompanied by stirring during the pre-concentration phase. For triple detection of Zn(II), AA, and PA, a potential of –1.6 V was applied for 5 min, again with stirring during pre-concentration. After a quiet time of 30 s, DPV and SWV measurements were conducted with the stirrer turned off, employing the following parameters: increment, 0.005 V; pulse amplitude, 0.05 V; and pulse width, 0.2 s. For DPV, the same parameters were used with an additional pulse period of 0.5 s. The potential range was set from –0.5 to 0.6 V for the simultaneous detection of 4-AP and PA, from –0.6 to 0.7 V for the simultaneous detection of AA and PA, and from –1.6 to 0.7 V for the triple detection of Zn(II), AA, and PA. The electrochemical impedance spectra (EIS) were measured over a frequency range of 100 KHz to 0.1 Hz with an amplitude of 10 mV in a 0.1 M KCl electrolyte with 0.5 mM $K_3[Fe(CN)_6]/K_4[Fe(CN)_6]$ (1:1).

2.4. Samples preparation

Three tablets of each chosen pharmaceutical product were carefully grinded in an agate mortar and precisely weighed. Their solutions were

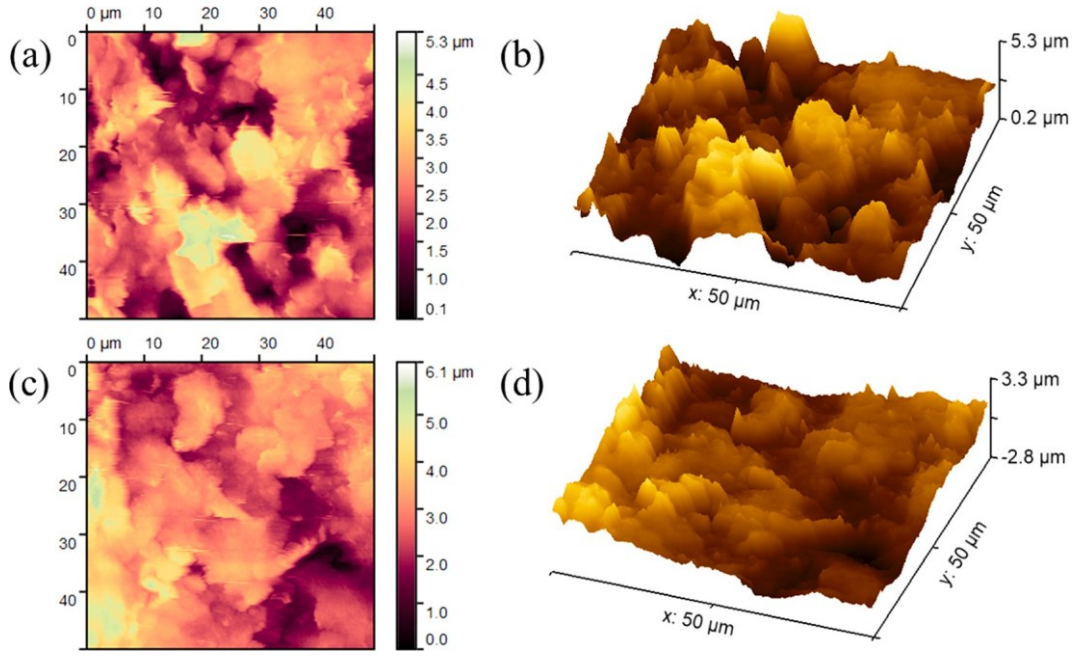

Fig. 2. (a) 2D, (b) 3D AFM images of SPE; (c) 2D, (d) 3D AFM images of Pt–Ni/SPE.

then made by ultrasonically dissolution in distilled water. Following centrifugation at 3500 rpm for 20 min, each resulting filtrate was gathered in a 50 ml graduated flask and further diluted with a 0.1 mol. L^{-1} buffer solution (either PBS or ABS, depending on the analyte). In the subsequent step, precise volumes of the resultant solutions were transferred to the electrolytic cell for SWV measurements. Notably, for the paracetamol sample, fortification with 4-AP was conducted prior to assay. The human blood serum samples of two healthy people were kindly provided by a local hospital. These samples were pretreated in compliance with our previous work [61].

3. Results and discussion

3.1. FE–SEM, TEM, EDX, XRD and AFM characterization of the surface modified SPEs

FE–SEM images of the modified electrode (Pt–Ni/SPE) prepared by simultaneous electrodeposition technique are illustrated in Fig. 1a. The surface morphology of SPE became homogeneous after the incorporation of highly uniform and well-dispersed Pt and Ni spherical particles. The high-magnification FE–SEM image (Inset Fig. 1a) reveals that many Pt nanodeposits were homogenously distributed throughout the substrate, with an average dimension up to ca. 300 nm. In contrast, only a few Ni nanoparticles with a smaller diameter were present. Within the experimental conditions outlined in this study, the electrodeposited Pt particles were found to be bigger in size compared to the Ni particles. Moreover, the TEM image of the modified electrode further proves its successful preparation (Fig. S2). The EDX spectrum of the as-fabricated Pt–Ni/SPE electrode (Fig. 1b) also presents elemental proof to confirm this result, with the atomic ratios of Pt and Ni were estimated to be about 97.17 % and 2.83 %, respectively. The high percentage of Pt particles compared to Ni particles is attributed to the fact that the highest electrocatalytic activity of platinum particles is achieved when the amount of nickel in the modified electrode is up to about 5 % [62]. The above results demonstrated the successful synthesis of Pt–Ni/SPE. Additionally, as illustrated in Fig. 1c, the crystal structure of Pt–Ni/SPE electrode was further examined by XRD. The peaks occurring in this figure at angular positions of 26.6°, 44.7°, and 54.8° belong to (002), (101), and (004) diffractions of hexagonal graphite (JCPDS No. 00–026–1080). Furthermore, three crystalline peaks were observed at 2θ values of 40.2°, 46.7°, and 68.2°, and which can be indexed to the (111), (200), and (220) diffractions of face-centered cubic of pure Pt (JCPDS No. 00–001–1194). In addition, other three characteristic peaks at 44.7°, 52.1°, and 76.6°, matches well with the (111), (200), and (220) crystalline planes of cubic phase Ni (JCPDS No. 00–004–0850). The XRD results also testified that Pt–Ni nanodeposits were formed and successfully loaded onto the graphite SPE electrode surface. Moreover, AFM analysis was performed on both unmodified and Pt–Ni modified SPE. Fig. 2a and b present two-dimensional (2D) and three-dimensional (3D) AFM images of the unmodified SPE, while Fig. 2c and d depict the 2D and 3D views of the Pt–Ni modified SPE, respectively. Comparing 3D AFM images in Fig. 2b and d reveals the relatively rough surface of the unmodified SPE, whereas the modified electrode surface appears moderately homogeneous, indicating the smooth distribution of Pt–Ni particles. This supports previous findings of successful Pt–Ni nanodeposits loading onto the graphite screen-printed electrode surface.

3.2. Electrochemical performance of the surface modified SPEs

To investigate the electrochemical behavior of the bare SPE, Pt/SPE and Pt–Ni/SPE through $Fe(CN)_6^{-3/-4}$ redox probe, CV and EIS analyses were performed in 0.1 M KCl solution containing 1.0 mM $Fe(CN)_6^{-3/-4}$ on the surface of these electrodes (Fig. S3). Fig. S3a illustrates the CVs of unmodified and modified SPEs, respectively. From this figure, it is found that the potential peak separation (ΔE_p) is 197 mV for the unmodified SPE, 133 mV for Pt/SPE, and 122 mV for Pt–Ni/SPE at a scan rate of 50 mV s^{-1}. The impact of Pt and Pt–Ni nanoparticles upon the SPE's heterogeneous electron transfer characteristics can be studied by employing Nicholson's method [63]. It is routinely used to estimate the heterogeneous electron transfer rate constant (k°) for quasi-reversible reactions using the following formula:

$$\psi = k^{\circ}[\pi D n \upsilon F/RT]^{-1/2} \quad (1)$$

where, ψ is a kinetic parameter, D is the diffusion coefficient ($D = 7.6 \times 10^{-6}$ cm^2 s^{-1} for $Fe(CN)^{-3/-4}$), υ is the voltammetric scanning rate, n is the number of electrons involved in the process, R, F, and T denote constants, with T is the temperature in Kelvin, R is the universal gas

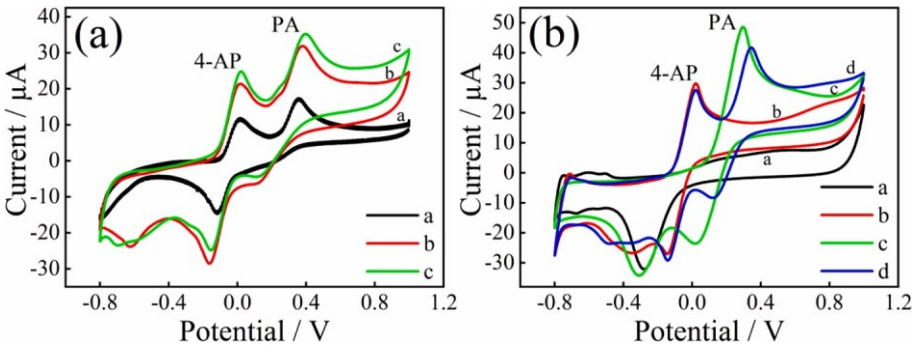

Fig. 3. (a) CVs of bare SPE (a), Pt/SPE (b), Pt–Ni/SPE (c) in PBS (0.1 M, pH = 7.4) containing a mixture of 300 μM 4-AP and PA. (b) CVs of the Pt–Ni/SPE electrode in 0.1 M PBS solution (pH = 7.4) without 4-AP and PA (a), with 300 μM 4-AP (b), 300 μM PA (c) and their mixture (d), respectively.

constant (8.314 J mol^{-1} K^{-1}), and F is the Faraday constant (96485.33 C mol^{-1}). ψ is deduced from (ΔE_p) at a set temperature (298 K) for a one-step, one electron process with the transfer coefficient α equal to 0.5. The function of ψ (ΔE_p), which fits Nicholson's data, for practical usage (rather than producing a working curve) is given by [64]:

$$\psi = (-0.6288 + 0.0021X)/(1 - 0.017X) \quad (2)$$

where $X = \Delta E_p$is used to determine ψ as a function of ΔE_p from the experimentally obtained voltammetric curves. From this, a plot of ψ against $[\pi DnuF/RT]^{-1/2}$ allows the k° to be readily determined. Using this approach, the corresponding k° values were estimated to be 2.4 × 10^{-4}, 5.3 × 10^{-4} and 5.9 × 10^{-4} for the unmodified SPE, Pt/SPE and Pt–Ni/SPE, respectively. Moreover, the redox peak currents observed over the various electrodes increased in the subsequent arrangement: SPE < Pt/SPE < Pt–Ni/SPE. Consequently, these changes demonstrate the electro-catalytic efficiency of Pt and Pt–Ni nanoparticles as modifiers, effectively enhancing and facilitating the electron transfer rate of the graphite SPE by factors of 2.2 and 2.5, respectively.

Electrochemical impedance spectra proved to be a powerful approach employed to investigate the interface characteristics of surface modified electrodes in the frequency ranging from 0.1 to 10^5 Hz. Fig. S3b shows the EIS typical spectra of the unmodified SPE, Pt/SPE and Pt–Ni/SPE, consisting of two parts, semicircle portion at higher frequencies, indicative of the electron transfer process with a diameter equal to the charge transfer resistance (R_{ct}), and a straight line at lower frequencies reflecting the diffusion control process [65].

The EIS spectra were theoretically fitted to a suitable equivalent circuit (as shown in Inset Fig. S3b), which is composed of solution resistance (R_1), Warburg simulating element (WS_1), charge transfer resistance (R_2) and the constant phase element (CPE_1). The fitted R_2 values for the bare SPE, Pt/SPE and Pt–Ni/SPE were found to be 6.99 KΩ (χ^2 = 0.0302), 2.68 KΩ (χ^2 = 0.0384) and 1.59 KΩ (χ^2 = 0.0385), respectively. Notably, the R_2 value reached its lowest for the Pt–Ni/SPE modified electrode, affirming its good electrical conductivity compared to the other electrodes. Hence, the EIS results were in agreement with both CV data and physical characterization results, demonstrating the effective modification of the screen-printed electrode surface with Pt–Ni nanoparticles.

The specific surface areas of bare SPE, Pt/SPE and Pt–Ni/SPE were calculated by CV method at different scan rates (Fig. S4) using *Rand- les–S˘ev˘cik* formula [66]:

$$I_p = \pm 0.436nFAC\sqrt{\frac{nFu}{RT}} \quad (3)$$

where, I_P is the anodic peak current (A), n is the number of electron transformed, A is the electroactive area of working electrode (cm^2), D is the diffusion coefficient (cm^2 s^{-1}), u is the scan rate (V s^{-1}) and C is the bulk concentration (mol cm^{-3}). Based on equation (3), the electroactive surface areas were determined to be 5.1 × 10^{-2}, 6.7 × 10^{-2} and 6.9 × 10^{-2} cm^2 for bare SPE, Pt/SPE and Pt–Ni/SPE, respectively. Thus, this result further confirms the successful growth of the Pt–Ni nanoparticles on the surface of the SPE electrode, leading to enhanced electroactive surface area of the modified electrode.

3.3. Electrochemical behaviors of 4-aminophenol and paracetamol at different modified electrodes

The electrochemical behaviors of 4-AP and PA were investigated on various modified electrodes (bare SPE, Pt/SPE and Pt–Ni/SPE) in 0.1 M PBS (pH = 7.4) containing 300 μM 4-AP and PA, respectively. The CV technique was employed for this analysis. As observed in Fig. 3a, the bare SPE depicted in the potential range of –0.8 to 1.0 V a pair of weak and broad redox peaks for 4-AP and PA (curve a). In comparison, the Pt/SPE exhibited an increase in the redox peak currents for both targets (curve b) by approximately 2 times, possibly due to the electro-catalytic activity of Pt particles.

Upon the surface modification of the Pt/SPE electrode through the co-deposition of Pt with Ni, as described in the experimental section, the oxidation peak currents density for both target analytes (curve c) exhibited a remarkable enhancement, surpassing that of the single metal modified electrode (Pt/SPE). This enhancement can be attributed to the abundant heterogeneous electron transfer properties of nickel particles, which further improved the sensing characteristics of the fabricated electrode by enhancing electrical conductivity of platinum particles. This assumption is in agreement with previously reported works on the oxidation of other analytes by the bi-metal (Pt–Ni) systems [67–69].

CV measurements were also used to study the electrochemical detection of 4-AP and PA individually and simultaneously using the Pt–Ni/SPE modified electrode. In Fig. 3b, the modified electrode was immersed in various solutions: blank PBS (a), 300 μM 4-AP (b), 300 μM PA (c) and their mixture solution (d). In the blank PBS solution (0.1 M, pH = 7.4), no redox peaks were observed, and only the characteristic signals associated with the Pt–Ni/SPE were present (curve a). When 4-AP was introduced, a pair of well-defined redox peaks, corresponding to the electrochemical behavior of 4-AP, appeared at 0.02 V for the anodic peak potential and –0.14 V for the cathodic peak potential (curve b). Subsequently, when the prepared Pt–Ni/SPE electrode was immersed in the PA solution, a pair of distinct redox peaks showed at 0.29 V and 0.02 V for anodic and cathodic peak potential, respectively (curve c), certainly corresponding to the electrochemical behavior of PA. As seen in curve d, the CV of the mixture containing both 4-AP and PA exhibited four distinct redox peaks related to the redox processes of 4-AP and PA, showing an anodic peak-to-peak separation up to 0.32 V. These data indicate that the redox peaks of 4-AP and PA are clearly separated, demonstrating the capability of the Pt–Ni/SPE modified electrode for the simultaneous and selective determination of these target species.

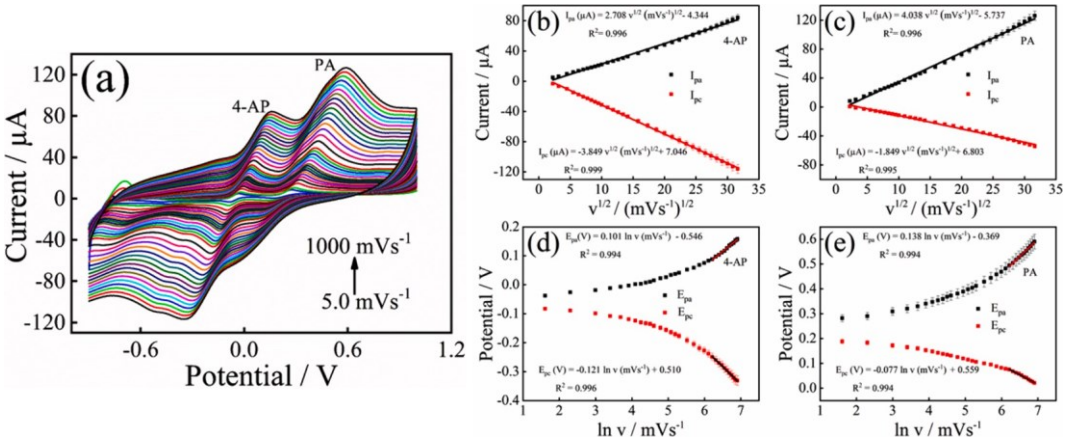

Fig. 4. (a) CVs of Pt–Ni/SPE electrode in 0.1 M PBS (pH 7.4) with a combination of 300 µM 4-AP and PA at various scan rates from 5.0 to 1000 mVs^{-1}, (b, c) Calibration plots of redox peak currents vs $\upsilon^{1/2}$, (d, e) Plots of redox peak potentials vs. $\ln\upsilon$. The error bars indicate the standard deviations of three repeated measurements.

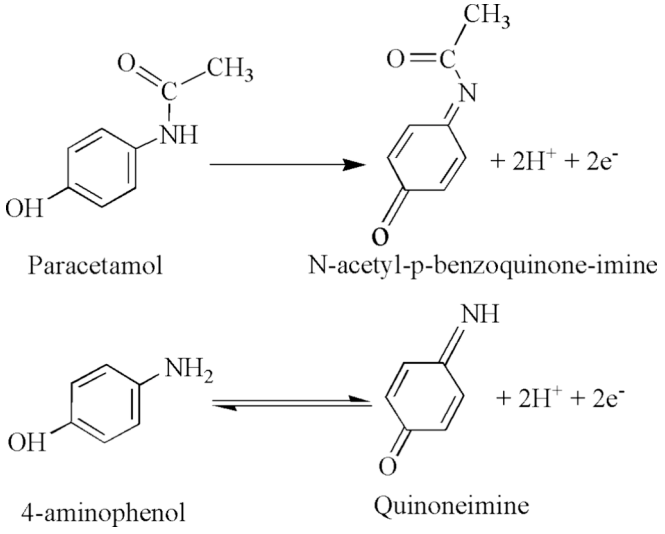

Scheme 1. Electrochemical reaction mechanism of 4-AP and PA on the Pt–Ni/SPE.

3.4. The pH value effect

The electrochemical oxidation of phenolic compounds to form quinone is fundamentally reliant on the process of proton transfer [70]. Consequently, variations in the buffer solution's pH can directly influence the electrochemical response of 4-AP and PA. Thus, the effect of the supporting electrolyte pH ranging between 6.0 and 9.0 on the redox response of 100 µM 4-AP and PA mixture at Pt–Ni/SPE with a scan rate of 50 mV s^{-1} was carried out by CV. As can be seen in Fig. S5a and b, as the pH value increases from 6.0 to 7.4, both the oxidation peak currents of 4-AP and PA exhibit a consistent increase. However, beyond this range, as the solution pH further increase, the oxidation peak currents decrease instead. Hence, pH 7.4 was selected for subsequent studies. Notably, at pH 6.0, we observed a strong current attributed to the hydrogen evolution reaction at the Pt surface; however, this current decreases for pH values above 6.0.

In Fig. S5c, it is evident that the E_{pa} values for 4-AP and PA exhibit a linear shift towards more negative directions as the pH increases within the range of 6.0 to 9.0. This is the indicative of the direct involvement of protons in the redox process of both 4-AP and PA [71]. The displayed regression equations are as follows: $E_{pa} = -0.058pH + 0.388 (R^2 = 0.99)$ and $E_{pa} = -0.05pH + 0.6$ $R^2 = 0.991$ for 4-AP and PA, respectively. Moreover, the slopes of the calibration curves, measuring 58.8 mV/pH for 4-AP and 50 mV/pH for PA, closely approximated the theoretical Nernstian value of 59 mV/pH [72]. This suggests that an equal number of protons and electrons had been participated in the oxidation–reduction mechanism of both phenolic analytes at the Pt–Ni/SPE modified electrode.

3.5. The scan rate influence

To provide more information about the charge transfer proprieties of 4-AP and PA, the impact of scan rate on the electrochemical reaction of 4-AP and PA at the surface of the Pt–Ni/SPE proposed electrode was examined through CV at various scan rates from 5.0 to 1000 mVs^{-1} using a concentration of 300 µM for both analytes. Fig. 4a reveals that as the scan rate increases, both 4-AP and PA electrochemical signals exhibit a gradual increase. At the same time, Fig. 4b and c shows that the anodic and cathodic peak currents (I_{pa} and I_{pc}) of the two phenolic compounds exhibited a proportional relationship with the square root of the scan rate ($\upsilon^{1/2}$). The fitting equations assumed for this relationship are as follows:

$$I_{pa}(\mu A) = 2.708\upsilon^{1/2}(mVs^{-1})^{1/2} - 4.344 \quad R^2 = 0.996$$

4—AP:

$$I_{pc}(\mu A) = -3.849\upsilon^{1/2}(mVs^{-1})^{1/2} + 7.046 \quad R^2 = 0.999$$

PA:

$$I_{pa}(\mu A) = 4.038\upsilon^{1/2}(mVs^{-1})^{1/2} - 5.737 \quad R^2 = 0.996$$

$$I_{pc}(\mu A) = -1.849\upsilon^{1/2}(mVs^{-1})^{1/2} + 6.803 \quad R^2 = 0.995$$

The phenomena clearly suggest that all electrochemical reactions at the surface of Pt–Ni/SPE modified electrode were diffusively controlled [73].

On the other hand, there is a slight positive and negative shift in the oxidation and reduction peak potentials (E_{pa} and E_{pc}) for these compounds as the scan rate increases, implying a kinetic limitation of the modified Pt–Ni/SPE towards 4-AP and PA oxidation. Fig. 4d and e shows the linear dependence between E_{pa}, E_{pc} and the natural logarithm of the scanning speed (lnυ). This linear relationship can be expressed through the following corresponding linear equations: $E_{pa}(V) = 0.101\ln\upsilon\ mVs^{-1}\ -0.546\ R^2 = 0.994$, $E_{pc}(V) = -0.121\ln\upsilon\ mVs^{-1}) + 0.510\ R^2 = 0.996)$ for 4-AP and $E_{pa}(V) = -0.369\ R^2 = 0.994$, $E_{pc}(V) = -0.077\ln\upsilon\ mVs^{-1}\ +0.559\ R^2 = 0.994$ for PA. Referring to Laviron's theory [74]:

)) $0.138\ln\upsilon\ mVs^{-1})$)))

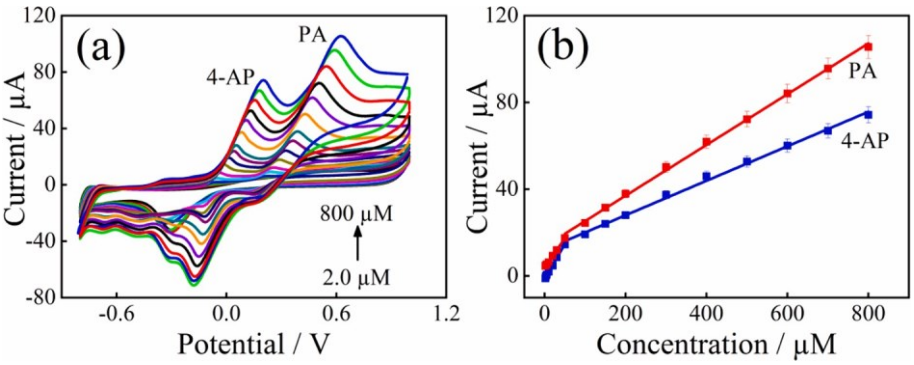

Fig. 5. (a) CVs of Pt–Ni/SPE for various concentrations of both 4-AP and PA (2.0–800 µM) in PBS (0.1 M, pH 7.4) at 50 mVs^{-1}. (b) Represents the plots of anodic peak currents vs. 4-AP and PA concentrations.

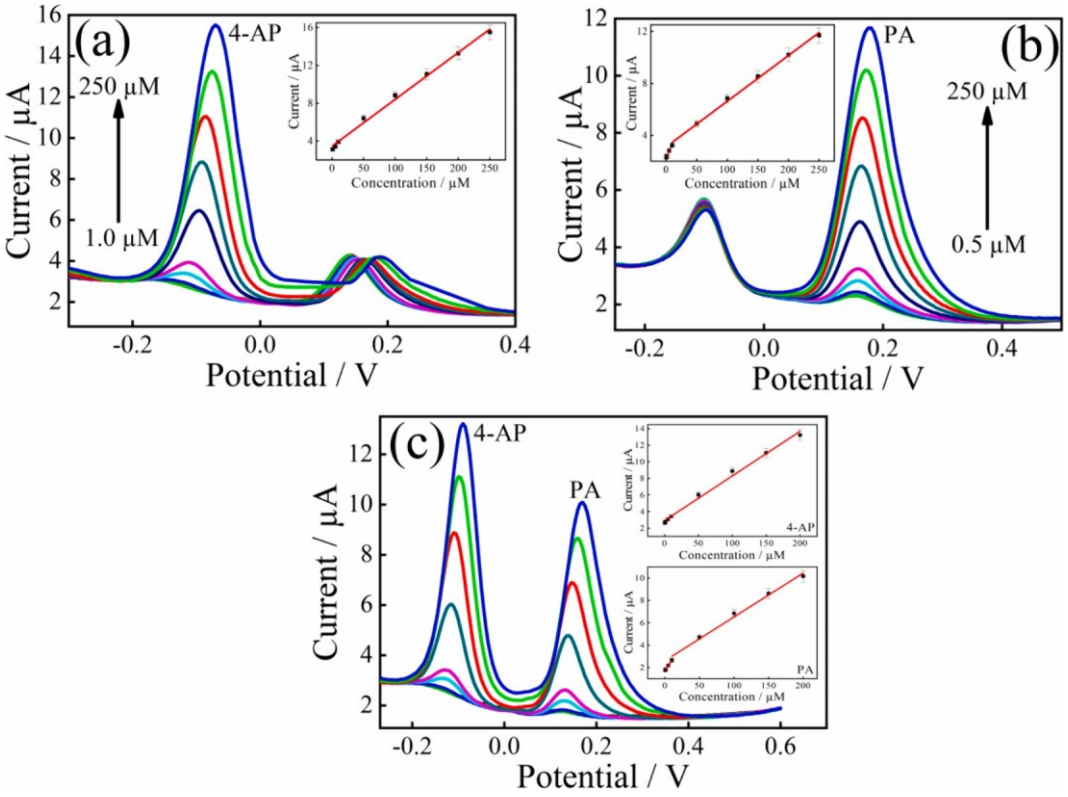

Fig. 6. DPV profiles of different mixtures of 4-AP and PA. (a) 4-AP (1.0–250 µM) and 40 µM PA, (b) PA (0.5–250 µM) and 40 µM 4-AP, (c) 4-AP and PA (0.5–200 µM) on Pt–Ni/SPE in 0.1 M PBS (pH = 7.4). The insets show the corresponding calibration curves.

$$E_{pa} = E^0 + Alnv \quad (4)$$

$$E_{pc} = E^0 + Blnv \quad (5)$$

$$A = \frac{RT}{(1-\alpha)nF} \text{ and } B = RT/\alpha nF$$

where all the constants remain consistent with the previous description, except for the standard redox potential E°. By analyzing the linear relationships between E_{pa}, E_{pc} and lnυ, it can be observed that the slopes of the linear regressions are equal to RT/αnF and RT/(1 —α)nF, respectively. Following the calculations, the values of n and α were found to be (2.45 and 0.47) for 4-AP and (2.41 and 0.55) for PA, respectively. Hence, the redox mechanism of the two phenolic compounds at the surface of our newly modified electrode involves the transfer of two electrons and two protons ($2\ e^{-}/2H^{+}$). The probable reaction mechanism of 4-AP and PA is described in Scheme 1, consistent with those previously reported [73,75].

3.6. Analytical features of Pt–Ni/SPE towards 4-aminophenol and paracetamol determination

CV and DPV methods were both performed to study the analytical performances of the developed electrochemical Pt–Ni/SPE sensor for the detection of 4-AP and PA. The concentration influence of 4-AP and PA at Pt–Ni/SPE was firstly tested by CV, as given in Fig. 5a. As can be seen, a good separation of 0.42 V is evident between the oxidation peaks of 4-AP and PA, where the current values for the oxidation of both compounds demonstrate a proportional increase corresponding to their respective concentrations. The linearity between the anodic peak current (I_{pa}) and concentration was demonstrated by plotting them against each other; as depicted in Fig. 5b. The plot clearly shows two distinct linear ranges for

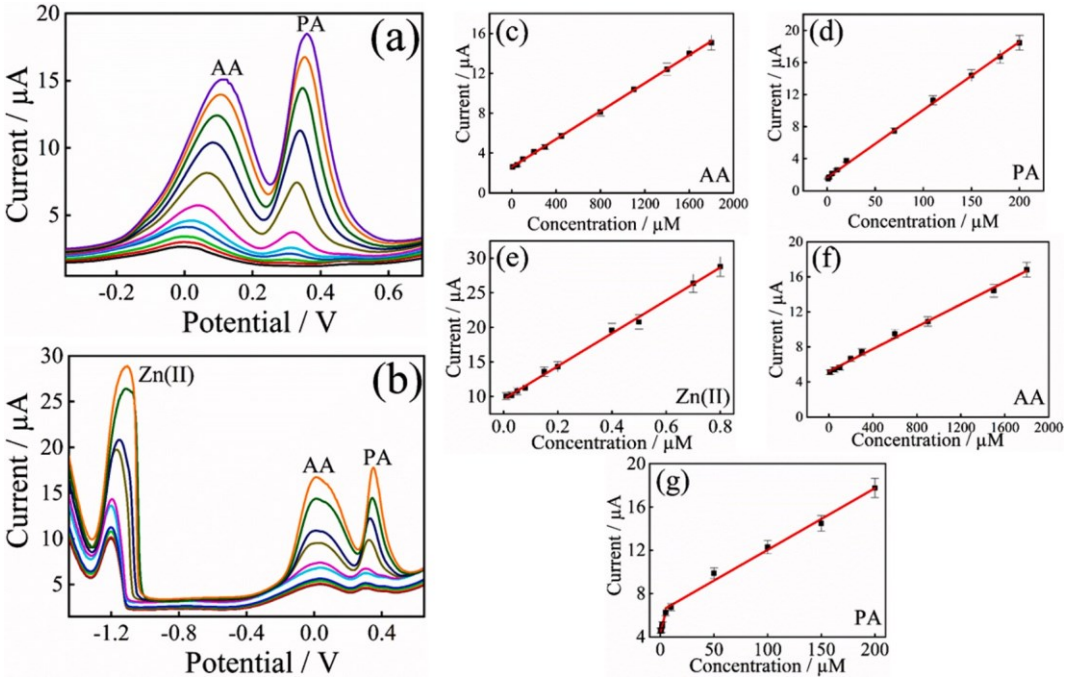

Fig. 7. SWV profiles at Pt–Ni/SPE in 0.1 M ABS (pH 4.7) containing a mixture of 10–1800 µM AA and 1.0–200 µM PA (a), and 0.01–0.8 µM Zn(II), 10–1800 µM AA and 0.5–200 µM PA (b). From c to g illustrate the corresponding calibration curves.

Table 1
Comparison of the fabricated Pt–Ni/SPE electrode's features with other related sensors reported in the literature for the detection of Zn(II), AA and PA.

Analyte	Electrode	Modifier	Technique	pH	Linear range (µM)	Detection limit (µM)	Ref.
Zn(II)	Screen-printed	Nafion/G/PANI[a]	SWASV	4.5	0.01–4.58	0.01	[77]
	Screen-printed carbon nanotubes	Bi[b]	SIA–ASV	4.0	0.18–1.52	0.17	[78]
	Carbon paste	$TbFeO_3$/CuO	SWASV	4.8	0.01–1.68	0.007	[23]
	Screen-printed carbon	PEDOT/PVA/AgNPs[c]	SWASV	4.6	0.15–1.22	0.09	[44]
	Glassy carbon	BiFE[d]	DP–ASV	4.5	0.07–1.68	0.016	[79]
	Screen-printed	Pt–Ni	SWV	4.7	0.01–0.8	0.004	This work
AA	Carbon fiber	GEF[e]	DPV	7.0	45.4–1489	24.70	[80]
	Glassy carbon	rGO–SnO_2	DPV	7.0	400–1600	38.70	[81]
	Carbon fiber paper	Pt@NP–AuSn/Ni	DPV	7.0	200–1200	13.4	[82]
	Glassy carbon	GS[f]	DPV	6.8	100–1000	100	[83]
	Glassy carbon	MLN[g]/Ag	Amp	7.0	30–1000	15	[84]
	Screen-printed	Pt–Ni	SWV	4.7	10–1800	9.0	This work
PA	Glassy carbon	MWCNTs/poly(Gly)[h]	DPV	7.0	0.5–10	0.5	[85]
	Carbon paste	CNT–P[i]	SWV	5.0	10–100	1.1	[86]
	Glassy carbon	MWCNT/GO/Poly(Thr)[j]	DPV	7.0	5.0–200	0.16	[87]
	Single walled carbon nanotube	AuNP–PGA[k]	DPV	7.2	8.3–145.6	1.18	[88]
	Carbon paste	NiCoSalenA[l]	DPV	3.0	1.71–137.6	0.51	[89]
	Screen-printed	Pt–Ni	SWV	4.7	0.5–200	0.15	This work

Key:
[a] G/PANI: graphene/polyaniline nanocomposite;
[b] Bi: bismuth;
[c] PEDOT/PVA/AgNPs: poly (3,4–ethylenedioxythiophene)/poly vinyl alcohol/silver nanoparticles;
[d] BiFE: bismuth film electrode;
[e] GEF: graphene flower;
[f] GS: graphene/SnO_2 nanocomposite;
[g] MLN: molybdenite;
[h] MWCNTs/ poly(Gly): multi–walled carbon nanotubes/poly (glycine);
[i] CNT–P: carbon nanotube/poly (3–aminophenol);
[j] GO/Poly(Thr): graphene oxide/poly (threonine);
[k] PGA: glutamic acid;
[l] NiCoSalenA: nickel–cobalt salen complexes/NaA nanozeolite.

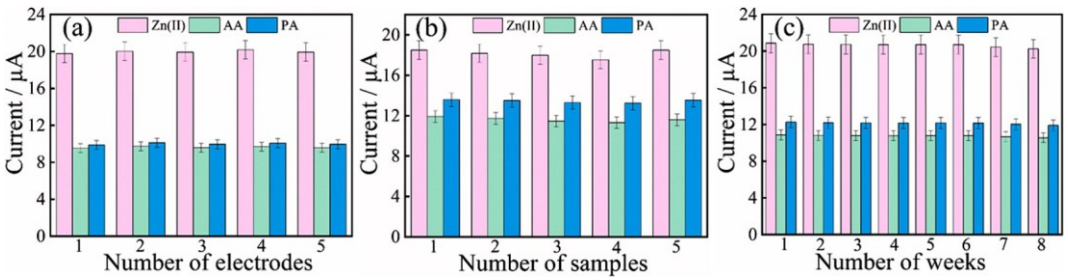

Fig. 8. (a) Reproducibility, (b) Repeatability and (c) Stability tests on Pt–Ni/SPE in the presence of a ternary mixture containing 0.6 μM Zn(II), 900 μM AA and 50 μM PA.

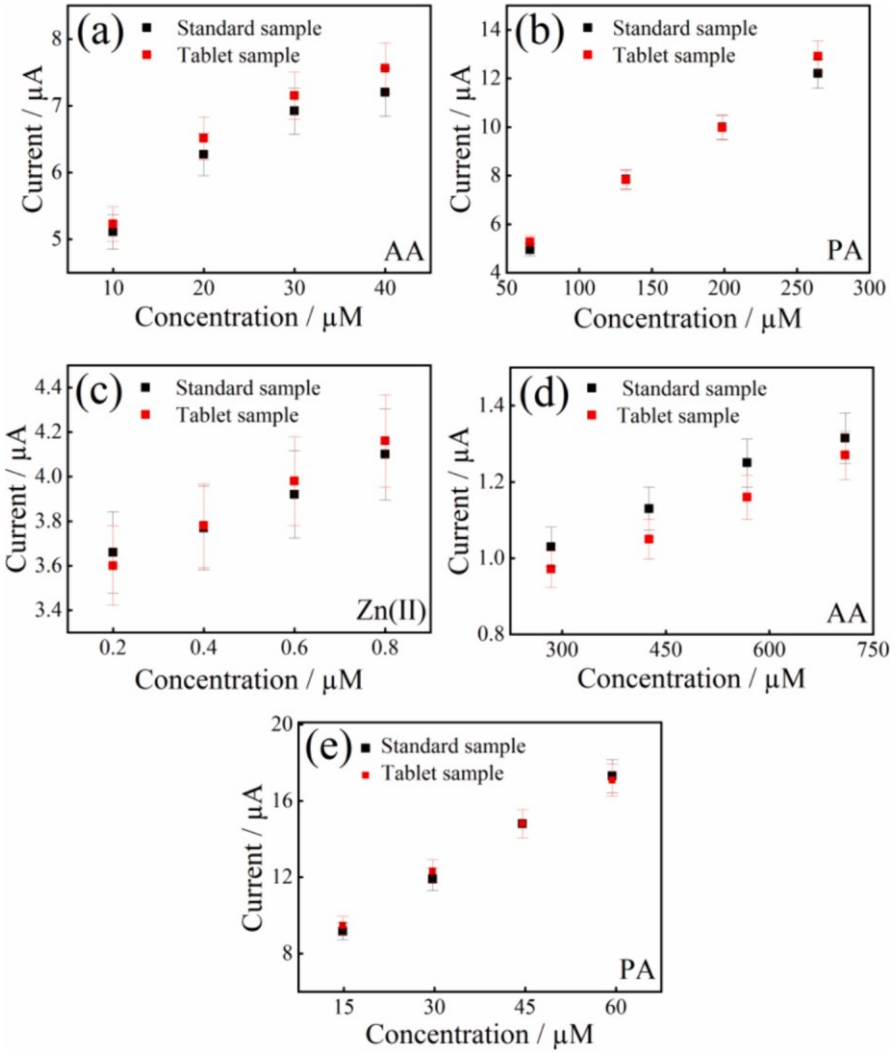

Fig. 9. (a–e) Sensor responses to identical analyte concentrations in tablet samples (red) vs. standard samples (black). (For interpretation of the references to colour in this figure legend, the reader is referred to the web version of this article.)

each analyte. The first range spans from 2.0 to 50 μM, and the subsequent range extends from 50 to 800 μM. Furthermore, the limits of detection (LODs) (S/N = 3) of the modified Pt–Ni/SPE towards the electro-oxidation process of the two target analytes were estimated as follows: 1.42 μM for 4-AP and 1.47 μM for PA, respectively. Their corresponding linear regression equations and correlation coefficients are listed in Table S1. According to these results, the developed Pt–Ni/SPE sensor can be used for the simultaneous detection of 4-AP and PA with high sensitivity.

The DPV method was also performed in PBS buffer pH 7.4 under optimal experimental conditions to investigate the electrochemical applicability of the recently developed Pt–Ni/SPE sensor for the individual as well as simultaneous determination of 4-AP and PA. Throughout the individual detection of the two target components within their combined solution, one component's concentration kept changing linearly, while the other maintained constant. In Fig. 6a, it is

Table 2
Results for the determination of 4-AP, PA, AA and Zn(II) in pharmaceutical tablet samples using Pt–Ni/SPE proposed sensor (n = 3).

Sample	Species	Reported content (mg per tablet)	Determined (mg per tablet	Recovery (%)	RSD (%) (n ¼ 3)
Efferalgan	PA	500	481	96.2	0.68
Vitamin C	AA	200	195.8	97.9	1.41
Vitamin C	Zn(II)	10	10.9	109	0.25
with Zinc	AA	250	263	105.2	2.89
Doliprane	PA	1000	987	98.7	0.94
	4-AP	ND	ND	—	—

ND: not detected.

evident that the DPV peak currents of 4-AP continue to exhibit a linear increase in response to varying concentrations ranging from 1.0 to 250 μM, while the peak currents and potentials of 40 μM PA remain relatively unchanged. The regression equation for 4-AP is derived as $I_p(\mu A) = 0.049C(\mu M) + 3.445(R^2 = 0.995)$, with a LOD of 0.95 μM (S/N = 3). Similarly, as depicted in Fig. 6b, when the 4-AP concentration is fixed at 40 μM, the oxidation peak current of PA demonstrates two linear ranges: one from 0.5 to 10 μM and another from 10 to 250 μM. The corresponding regression equations are $I_p(\mu A) = 0.097C(\mu M) + 2.280(R^2 = 0.994)$ and $I_p(\mu A) = 0.035C(\mu M) + 3.103(R^2 = 0.996)$, respectively. Using the first linear fitting equation, the corresponding LOD was determined to be 0.25 μM (S/N = 3). These results undeniably demonstrate that the addition of one component has minimal impact on the detection of the other.

In a subsequent step, the Pt–Ni/SPE was used for the simultaneous detection of 4-AP and PA by changing their concentrations synchronously (Fig. 6c). As evident, the peak-to-peak separation of 0.26 V is sufficiently enough for the simultaneous determination of 4-AP and PA. Moreover, their oxidation peak currents displayed good linear relationships as their concentrations were gradually increased. The corresponding linear equations are depicted as follows:

$I_p(\mu A) = 0.053C(\mu M) + 2.912(0.5 — 200\mu M, R^2 = 0.992)$ for 4-AP, and $I_p(\mu A) = 0.089C(\mu M) + 1.734(0.5 — 10\mu M, R^2 = 0.998)$, $I_p(\mu A) = 0.039C(\mu M) + 2.611\ \ 10 — 200\mu M, R^2 = 0.991)$ for PA. The determined LOD and sensitivity values of the newly modified Pt–Ni/SPE for 4-AP and PA detection were 0.33 μM, $0.768 \pm 0.01 \mu A \mu M^{-1} cm^{-2}$ and 0.23μM, $1.289 \pm 0.01 \mu A \mu M^{-1} cm^{-2}$ correspondingly. Based on these results, individual or simultaneous determination of 4-AP and PA on Pt–Ni/SPE can be realized with high sensitivity and selectivity.

Similar to the findings in previous CV results where both analytes displayed two linear ranges, Fig. 6b and c also reveal that PA exhibits two linear ranges, possibly attributed to the following causes. In the case of low PA concentrations, the modified electrode had a surplus of available active sites that swiftly reacted with PA as the analyte, leading to a rapid current response. On the other hand, at higher levels of PA, it is possible that the electrode became contaminated due to the presence of the analytes and their resultant substances, resulting in a decrease in the sensitivity of the electrode [76]. In comparison to some previous reports in the literature for 4-AP and PA simultaneous detection, our newly Pt–Ni/SPE sensor developed in this work offers several advantages such as a widest linear range, lower detection limit and higher sensitivity, as shown in Table S2. These results highlight the immense potential of our novel electrode as a compelling candidate for the simultaneous determination of 4-AP and PA.

3.7. Simultaneous determination of ascorbic acid and paracetamol

Simultaneous analysis of AA and PA at the modified Pt–Ni/SPE electrode was further performed. Fig. 7a illustrates the SWVs for the concurrent addition of different concentrations of AA and PA in 0.1 M acetate buffer (ABS, pH 4.7). The presence of two well-defined oxidation peaks is clearly evident in the data at potential values of 0.11 V and 0.36 V, corresponding to AA and PA, respectively. The observed peak-to-peak separation of 0.25 V is sufficient for the simultaneous quantification of both above species, analogous to the prior determination of 4-AP and PA conducted simultaneously. In addition, there was a good linear correlation observed between the concentrations of AA and PA and their respective oxidation peak currents. The corresponding linear regression equations are as follows (see Fig. 7c and d):

AA : $I_p(\mu A) = 0.007C(\mu M) + 2.586(10 — 1800\mu M, R^2 = 0.999)$

PA : $I_p(\mu A) = 0.085C(\mu M) + 1.631\ \ 1.0 — 200\mu M, R^2 = 0.998)$,

with the calculated LODs were 7.0 μM and 0.66 μM (S/N = 3) for AA and PA, respectively.

3.8. Simultaneous determination of zinc, ascorbic acid and paracetamol

Under the optimal conditions, Pt–Ni/SPE proposed electrode was also employed for the simultaneous quantification of three analytes. Fig. 7b displays the recorded SWVs for a ternary mixture solution comprising varying concentrations of Zn(II), AA, and PA in 0.1 M ABS (pH 4.7). As can be seen, each analyte in the mixture displayed distinct oxidation current peaks, and there is a proportional increase in oxidation peak current intensities as the concentrations of all analytes increase. The corresponding regression equations were expressed as (see Fig. 7e–g):

Zn(II) : $I_p(\mu A) = 23.816C(\mu M) + 9.620(0.01 — 0.8\mu M, R^2 = 0.997)$

AA : $I_p(\mu A) = 0.006C(\mu M) + 5.213(10 — 1800\mu M, R^2 = 0.996)$

PA : $I_p(\mu A) = 0.388C(\mu M) + 4.322\ \ 0.5 — 5.0\mu M, R^2 = 0.995)$
$I^p(\mu A) = 0.0569C(\mu M) + 6.350\ \ 5.0 — 200\mu M, R^2 = 0.992)$,

The two linear ranges of PA are probably due to the fact that the sensor starts oxidizing Zn(II) and AA first. It is also noteworthy that the sensor exhibits an excellent separation of the detection potential of Zn (II) from that of AA and PA, with an inter-peak potential difference of 1.12 V. This provides the opportunity of detecting of other electroactive analytes within this range. The estimated LODs values for Zn(II), AA and PA were determined as follows: 0.004 μM; 9.0 μM; and 0.15 μM;

Table 3
The obtained recovery values of Zn(II), AA, and PA in human plasma samples.

Sample	Analyte (μM)						Recovery (%)		
	Added			Found					
	Zn(II)	AA	PA	Zn(II)	AA	PA	Zn(II)	AA	PA
Serum 1	0	0	0	ND	ND	ND	—	—	—

	0.15	1000	100	0.14	1033	95.6	96.1	103.5	95.8
Serum 2	0	0	0	ND	ND	ND	—	—	—
	0.10	500	50	0.098	489	47.7	98	97.8	95.4

respectively. The outcomes show that this constructed electrode as a sensor is capable of effectively detecting Zn(II), AA, and PA simultaneously in a single analytical run. When compared to various sensors reported in previous studies (Table 1), this sensor exhibits satisfactory linear ranges and detection limits for the target analytes.

3.9. Reproducibility, repeatability and stability effect

In order to evaluate the fabrication reproducibility of Pt–Ni/SPE, five modified electrodes were prepared under identical conditions to simultaneously determine 0.6 μM Zn(II), 900 μM AA and 50 μM PA (see Fig. 8a). The relative standard deviation (RSD) of the SWV response was 4.0 % for Zn(II), 2.3 % for AA, and 1.5 % for PA, separately, indicating that the Pt–Ni/SPE possessed outstanding fabrication reproducibility.

Moreover, the repeatability of the developed electrode was also investigated using a single Pt–Ni/SPE electrode for five successive measurements in ABS samples containing the same ternary mixture (see Fig. 8b) and the RSD values for Zn(II), AA and PA were 1.5 %, 1.1 % and 1.2 %, respectively, confirming the decent repeatability of the fabricated sensor.

To measure the long term stability of the proposed modified electrode, Pt–Ni/SPE was stored at room temperature for 8 weeks, and only a slight decrease in the oxidation peak currents of Zn(II), AA and PA was observed (see Fig. 8c), with reductions of around 2.92 %, 2.85 % and 3.0 % of the initial SWV responses respectively, clarifying the excellent long- term stability of the modified electrode.

3.10. Interference studies

The selectivity of the Pt–Ni/SPE fabricated sensor was also investigated by adding potential foreign substances commonly found in food, beverages, or possibly present in pharmaceutical tablets. These substances comprised diverse ions and organic substances, including but not limited to Na^+, K^+, Cl^-, SO_4^{2-}, caffeine, glucose, fructose and galactose. Additionally, examination included physiological interfering compounds, such as citric acid. All of these substances may exist in similar environment with the target analytes. As presented in Fig. S6, 1.0 mM of Na^+, K^+, Cl^-, SO_4^{2-}, Caf, Cit, and 0.5 mM of Glu, Fru, and Gal did not affect the oxidation signals of 0.6 μM Zn(II), 900 μM AA and 50 μM PA (changes in signal remained under 10 %). The results demonstrated that the Pt–Ni/SPE sensor had no interfering ability and good selectivity toward Zn(II), AA and PA simultaneous detection.

3.11. Analytical applications in pharmaceutical tablet and blood samples: Assessing sensor feasibility and practical applicability

The feasibility of the designed electrochemical sensor was evaluated using both pharmaceutical tablet samples and corresponding standard samples with identical analyte concentrations. Specifically, the pharmaceutical tablet samples included Efferalgan Vitamin C tablet (200 mg AA + 500 mg PA), a Vitamin C with Zinc complementary dietary supplement (10 mg Zn(II) + 250 mg AA), and Doliprane tablet (1000 mg PA).

As shown in Fig. 9, the Pt–Ni/SPE modified electrode exhibited consistent current responses across all sample types, indicating its robust performance. This suggests its potential suitability for real applications.

To further validate the practical utility of the Pt–Ni/SPE sensor, the concentrations of various analytes in the aforementioned pharmaceutical tablets were determined using the standard addition method, facilitated by SWV technique under optimized conditions. The obtained results were summarized in Table 2 and the samples pre-treatment process is detailed in Section 2.4. It can be seen that the determination results were in quite agreement with the specified target contents given by the manufacturer with the recoveries ranged from 96.2 to 109 %. In addition, the RSD values of each sample for three time's parallel detections were less than 2.89 %. It is noteworthy that the additives contained in the tablets did not exhibit any interference effect on the determination of analytes in the commercial samples. These results illustrated that the Pt–Ni/SPE developed sensor possessed reliability and accuracy in the determination of PA, AA and Zn(II) in pharmaceutical tablets.

Furthermore, recovery experiments for the simultaneous determination of Zn(II), AA, and PA in human serum samples were conducted using the same parameters as those employed in the SWV experiment with the Pt–Ni/SPE sensor. Certain amounts of Zn(II), AA and PA were spiked in human serum sample, and the analysis results were listed in Table 3. The recovery rates were in the range of 95.4–103.5 % and the correlation standard deviation is less than 4 %. The results prove that the Pt–Ni/SPE has great potential for the detection of Zn(II), AA and PA in practical serum.

4. Conclusion

In summary, a novel and effective electrochemical strategy is developed for the simultaneous detection of paracetamol in the presence of its toxic impurities (4-aminophenol) or its commonly co-formulated drugs (ascorbic acid and zinc) in pharmaceutical formulations and human blood samples, employing a pioneering Pt–Ni/SPE sensor coupled with DPV and SWV techniques. The electrodeposition technique formed a bimetallic sensor architecture with Pt and Ni nanodeposits, showcasing outstanding electrochemical properties (rapid electron transfer kinetics and a large electroactive surface area). In terms of simultaneous detection, the designed Pt–Ni/SPE sensor displayed exceptional electro-catalytic activity for 4-AP, PA, AA and Zn(II) electrochemical sensing, offering compelling sensitivity, low limits of detection, and a wide linear range, making it highly suitable for sensor applications. Leveraging a dual-effect approach, the sensor efficiently detects Zn(II) through Pt and 4-AP, AA, and PA through Pt–Ni. Additionally, the sensor is capable of effectively separating the detection potentials of Zn(II), AA, and PA, with a 1.12 V inter-peak difference, allowing the detection of other electroactive analytes within this range. Overall, the Pt–Ni/SPE sensor demonstrated excellent sensitivity, stability, repeatability, and reproducibility, with minimal interference observed in target analytes detection, as confirmed by interference studies. Therefore, the sensor effectively analyzed PA, 4-AP, AA, and Zn (II) in pharmaceutical and human blood samples, yielding satisfactory recovery rates.

CRediT authorship contribution statement

Fatima Zahra Makhlouf: Writing – original draft, Visualization, Validation, Methodology, Investigation, Formal analysis, Data curation, Conceptualization. **Mohamed Lyamine Chelaghmia:** Writing – review & editing, Visualization, Validation, Supervision, Methodology, Investigation, Formal analysis, Data curation, Conceptualization. **Rafiaa Kihal:** Formal analysis, Data curation. **Craig E. Banks:** Visualization, Validation, Data curation. **Hassina Fisli:** Methodology, Formal analysis. **Mouna Nacef:** Supervision, Formal analysis. **Abed Mohamed Affoune:** Validation, Methodology, Formal analysis. **Maxime Pontie´:** Visualization, Validation, Formal analysis.

Declaration of competing interest

The authors declare that they have no known competing financial interests or personal relationships that could have appeared to influence the work reported in this paper.

Data availability

Data will be made available on request.

Acknowledgement

We are very grateful to the financial support within the General Direction of Scientific Research and Technology Development of the Algerian ministry of higher education and scientific research.

References

[1] H. Wang, S. Zhang, S. Li, J. Qu, Electrochemical sensor based on palladium-reduced graphene oxide modified with gold nanoparticles for simultaneous determination of acetaminophen and 4-aminophenol, Talanta 178 (2018) 188–194.

[2] R.M. Hanabaratti, S.M. Tuwar, S.T. Nandibewoor, J.I. Gowda, Fabrication and characterization of zinc oxide nanoparticles modified glassy carbon electrode for sensitive determination of paracetamol, Chem. Data Coll. 30 (2020) 100540.

[3] N. Dou, J. Qu, Rapid synthesis of a hybrid of rGO/AuNPs/MWCNTs for sensitive sensing of 4-aminophenol and acetaminophen simultaneously, Anal. Bioanal. Chem. 413 (2021) 813–820.

[4] M. Khairy, B.G. Mahmoud, C.E. Banks, Simultaneous determination of codeine and its co-formulated drugs acetaminophen and caffeine by utilising cerium oxide nanoparticles modified screen-printed electrodes, Sens. Actuators B Chem. 259 (2018) 142–154.

[5] T.T. Calam, Selective and sensitive determination of paracetamol and levodopa with using electropolymerized 3,5-diamino-1,2,4-triazole film on glassy carbon electrode, Electroanal. 33 (2021) 1049–1062.

[6] M. Palanna, I. Mohammed, S. Aralekallu, M. Nemakal, L.K. Sannegowda, Simultaneous detection of paracetamol and 4-aminophenol at nanomolar levels using biocompatible cysteine–substituted phthalocyanine, New J. Chem. 44 (2020) 1294–1306.

[7] N. Dou, S. Zhang, J. Qu, Simultaneous detection of acetaminophen and 4-amino-phenol with an electrochemical sensor based on silver–palladium bimetal nanoparticles and reduced graphene oxide, RSC Adv. 9 (2019) 31440–31446.

[8] M. Kenarkob, Z. Pourghobadi, Electrochemical sensor for acetaminophen based on a glassy carbon electrode modified with ZnO/Au nanoparticles on functionalized multi-walled carbon nano-tubes, Microchem. J. 146 (2019) 1019–1025.

[9] F.Y. Kong, S.X. Gu, J.Y. Wang, H.L. Fang, W. Wang, Facile green synthesis of graphene–titanium nitride hybrid nanostructure for the simultaneous determination of acetaminophen and 4-aminophenol, Sens. Actuators B Chem. 213 (2015) 397–403.

[10] K. Alanazi, A.G. Cruz, S.D. Masi, A. Voorhaar, O.S. Ahmad, T. Cowen, E. Piletska, N. Langford, T.J. Coats, M.R. Sims, S.A. Piletsky, Disposable paracetamol sensor based on electroactive molecularly imprinted polymer nanoparticles for plasma monitoring, Sens. Actuators B Chem. 329 (2021) 129128.

[11] Y. Dong, M. Zhou, L. Zhang, 3D multiporous Co, N co-doped Mo_O2/MoC nanorods hybrids as improved electrode materials for highly sensitive simultaneous determination of acetaminophen and 4-aminophenol, Electrochim. Acta 302 (2019) 56–64.

[12] M. Nemakal, S. Aralekallu, I. Mohammed, M. Pari, K.R.V. Reddy, L.K. Sannegowda, Nanomolar detection of 4-aminophenol using amperometric sensor based on a novel phthalocyanine, Electrochim. Acta 318 (2019) 342–353.

[13] T.T. Calam, A modified pencil graphite electrode with 2-thiobarbituric acid for the efficient and cheap voltammetric sensing of 4-aminophenol in water samples and child syrup sample, J. Food Compos. Anal. 98 (2021) 103809.

[14] L. Suntornsuk, W. Gritsanapun, S. Nilkamhank, A. Paochom, Quantitation of vitamin C content in herbal juice using direct titration, J. Pharm. Biomed. Anal. 28 (2002) 849–855.

[15] F. Shayanfar, H. Sarhadi, Determination of vitamin C at modified screen printed electrode: application for sensing of vitamin c in real samples, Surf. Eng. Appl. Electrochem. 57 (2021) 487–494.

[16] G.E. Uwaya, O.E. Fayemi, Electrochemical detection of ascorbic acid in orange on iron(III) oxide nanoparticles modified screen printed carbon electrode, J. Clust. Sci. 33 (2022) 1035–1043.

[17] S. Liu, X. Jiang, M. Yang, Electrochemical sensing of L-ascorbic acid by using a glassy carbon electrode modified with a molybdophosphate film, Microchim. Acta 186 (2019) 445.

[18] M.A. Kumar, V. Lakshminarayanan, S.S. Ramamurthy, Platinum nanoparticles-decorated graphene-modified glassy carbon electrode toward the electrochemical determination of ascorbic acid, dopamine, and paracetamol, C. R. Chim. 22 (2019) 58–72.

[19] G. Kuntoji, N. Kousar, S. Gaddimath, L.K. Sannegowda, Macromolecule–nanoparticle-based hybrid materials for biosensor applications, Biosensors 14 (2024) 277.

[20] Y. Ma, Y. Zhang, L. Wang, An electrochemical sensor based on the modification of platinum nanoparticles and ZIF-8 membrane for the detection of ascorbic acid, Talanta 226 (2021) 122105.

[21] T. Kambe, K.M. Taylor, D. Fu, Zinc transporters and their functional integration in mammalian cells, J. Biol. Chem. 296 (2021) 100320.

[22] G. Ringgit, S. Siddiquee, S. Saallah, M.T.M. Lal, A sensitive and rapid determination of zinc ion (Zn^{2+}) using electrochemical sensor based on f-MWCNTs/CS/PB/AuE in drinking water, Sci. Rep. 12 (2022) 18582.

[23] H.M. Moghaddam, M. Amiri, H.A. Javar, Q.A. Yousif, M.S. Niasari, Green synthesis and characterization of Tb-Fe-O-Cu ceramic nanocomposite and its application in simultaneous electrochemical sensing of zinc, cadmium and lead, Arab. J. Chem. 15 (2022) 103988.

[24] Y. Shao, Y. Dong, L. Bin, L. Fan, L. Wang, X. Yuan, D. Li, X. Liu, S. Zhao, Application of gold nanoparticles/polyaniline-multi-walled carbon nanotubes modified screen-printed carbon electrode for electrochemical sensing of zinc, lead, and copper, Microchem. J. 170 (2021) 106726.

[25] C.T. Chasapis, P.S.A. Ntoupa, C.A. Spiliopoulou, M.E. Stefanidou, Recent aspects of the effects of zinc on human health, Arch. Toxicol. 94 (2020) 1443–1460.

[26] Y. Ai, L. Yan, S. Zhang, X. Ye, Y. Xuan, S. He, X. Wang, W. Sun, Ultra-sensitive simultaneous electrochemical detection of Zn(II), Cd(II) and Pb(II) based on the bismuth and graphdiyne film modified electrode, Microchem. J. 184 (2023) 108186.

[27] S. Thomas, D. Patel, B. Bittel, K. Wolski, Q. Wang, A. Kumar, Z.J. Il'Giovine, R. Mehra, C. McWilliams, S.E. Nissen, M.Y. Desai, Effect of high-dose zinc and ascorbic acid supplementation vs usual care on symptom length and reduction among ambulatory patients with SARS-CoV-2 infection, JAMA Netw. Open 4 (2021).

[28] Z. Wang, S. Cui, S. Qiu, S. Pu, A dual-functional fluorescent sensor based on diarylethene for Zn^{2+} and Al^{3+} in different solvents, J. Photochem. Photobiol. A Chem. 376 (2019) 185–195.

[29] T. Belal, T. Awad, C.R. Clark, Determination of paracetamol and tramadol hydrochloride in pharmaceutical mixture using HPLC and GC-MS, J. Chromatogr. Sci. 47 (2009) 849–854.

[30] Q. Chu, L. Jiang, X. Tian, J. Ye, Rapid determination of acetaminophen and p-aminophenol in pharmaceutical formulations using miniaturized capillary electrophoresis with amperometric detection, Anal. Chim. Acta 606 (2008) 246–251.

[31] S. Cheemalapati, S. Palanisamy, V. Mani, S.M. Chen, Simultaneous electrochemical determination of dopamine and paracetamol on multiwalled carbon nanotubes/graphene oxide nanocomposite-modified glassy carbon electrode, Talanta 117 (2013) 297–304.

[32] S.Z. Mohammadi, H. Beitollahi, M. Jasemi, A. Akbari, Nanomolar determination of methyldopa in the presence of large amounts of hydrochlorothiazide using a carbon paste electrode modified with graphene oxide nanosheets and 3-(4'-amino-3'-hydroxy-biphenyl-4-yl)- acrylic acid, Electroanalysis 27 (2015) 242–2430.

[33] S. Tajik, M.A. Tahar, H. Beitollahi, The first electrochemical sensor for determination of mangiferin based on an ionic liquid–graphene nanosheets paste electrode, Ionics 20 (2014) 1155–1161.

[34] S. Tajik, Z. Dourandish, F.G. Nejad, H. Beitollahi, P.M. Jahani, A.D. Bartolomeo, Transition metal dichalcogenides: synthesis and use in the development of electrochemical sensors and biosensors, Biosens. Bioelectron. 216 (2022) 114674.

[35] V.A. Sajjan, I. Mohammed, M. Nemakal, S. Aralekallu, K.K.R. Hemantha, S. Swamy, L.K. Sannegowda, Synthesis and electropolymerization of cobalt tetraaminebenzamidephthalocyanine macrocycle for the amperometric sensing of dopamine, J. Electroanal. Chem. 838 (2019) 33–40.

[36] J.P. Metters, R.O. Kadara, C.E. Banks, New directions in screen printed electroanalytical sensors: an overview of recent developments, Analyst 136 (2011) 1067.

[37] B. Thakur, E. Bernalte, J.P. Smith, C.W. Foster, P.E. Linton, S.N. Sawant, C. E. Banks, Utilising copper screen-printed electrodes (CuSPE) for the electroanalytical sensing of sulfide, Analyst 141 (2016) 1233.

[38] A.A. Khorshed, M. Khairy, C.E. Banks, Electrochemical determination of antihypertensive drugs by employing costless and portable unmodified screen-printed electrodes, Talanta 198 (2019) 447–456.

[39] E.P. Randviir, D.A.C. Brownson, J.P. Metters, R.O. Kadara, C.E. Banks, The fabrication, characterisation and electrochemical investigation of screen-printed graphene electrodes, PCCP 16 (2014) 4598–4611.

[40] P.M. Jahani, S.Z. Mohammadi, A. Khodabakhshzadeh, J.H. Cha, M.S. Asl, M. Shokouhimehr, K. Zhang, Q.V. Le, W. Peng, Simultaneous detection of morphine and diclofenac using graphene nanoribbon modified screen-printed electrode, Int. J. Electrochem. Sci. 15 (2020) 9037–9048.

[41] H. Beitollahi, M. Shahsavari, I. Sheikhshoaie, S. Tajik, P.M. Jahani, S. Z. Mohammadi, A.A. Afshar, Amplified electrochemical sensor employing screen-printed electrode modified with Ni–ZIF–67 nanocomposite for high sensitive analysis of sudan I in present bisphenol A, Food Chem. Toxicol. 161 (2022) 112824.

[42] A. Jirasirichote, E. Punrat, A.S. Ngam, O. Chailapakul, S. Chuanuwatanakul, Voltammetric detection of carbofuran determination using screen-printed carbon electrodes modified with gold nanoparticles and graphene oxide, Talanta 175 (2017) 331–337.

[43] S. Tajik, H. Beitollahi, S. Shahsavari, F.G. Nejad, Simultaneous and selective elechtrochemical sensing of methotrexate and folic acid in biological fluids and pharmaceutical samples using Fe_3O_4/ppy/Pd nanocomposite modified screen printed electrode, Chemosphere 291 (2022) 132736.

[44] U. Ngoensawat, T. Pisuchpen, Y. Sritana-anant, N. Rodthongkum, V.P. Hoven, Conductive electrospun composite fibers based on solid-state polymerized Poly (3,4-ethylenedioxythiophene) for simultaneous electrochemical detection of metal ions, Talanta 241 (2022) 123253.

[45] B. Patella, A. Sortino, F. Mazzara, G. Aiello, G. Drago, C. Torino, A. Vilasi, A. O'Riordan, R. Inguanta, Electrochemical detection of dopamine with negligible

interference from ascorbic and uric acid by means of reduced graphene oxide and metals-NPs based electrodes, Anal. Chim. Acta 1187 (2021) 339124.
[46] W. Liu, Q. Chen, Y. Huang, D. Wang, L. Li, Z. Liu, In situ laser synthesis of Pt nanoparticles embedded in graphene films for wearable strain sensors with ultra-high sensitivity and stability, Carbon 190 (2022) 245–254.
[47] Y. Chen, Q. Li, H. Jiang, X. Wang, Pt modified carbon fiber microelectrode for electrochemically catalytic reduction of hydrogen peroxide and its application in living cell H_2O_2 detection, J. Electroanal. Chem. 781 (2016) 233–237.
[48] M. Nacef, M.L. Chelaghmia, O. Khelifi, M. Ponti´e, M. Djelaibia, R. Guerfa, V. Bertagna, C. Vautrin-Ul, A. Fares, A.M. Affoune, Electrodeposited Ni on pencil graphite electrode for glycerol electrooxidation in alkaline media, Int. J. Hydrogen Energ. 46 (2021) 37670–37678.
[49] M.L. Chelaghmia, M. Nacef, H. Fisli, A.M. Affoune, M. Ponti´e, A. Makhlouf, T. Derabla, O. Khelifi, F. Aissat, Electrocatalytic performance of Pt–Ni nanoparticles supported on an activated graphite electrode for ethanol and 2–propanol oxidation, RSC Adv. 10 (2020) 36941–36948.
[50] R. Zhu, Z. Zhao, J. Cao, H. Li, L. Ma, K. Zhou, Z. Yu, Q. Wei, Effect of Pt–Ni deposition sequence on the bimetal-modified boron-doped diamond on catalytic performance for glucose oxidation in neutral media, J. Electroanal. Chem. 907 (2022) 116084.
[51] M.L. Chelaghmia, H. Fisli, M. Nacef, D.A.C. Brownson, A.M. Affoune, H. Satha, C. E. Banks, Disposable non-enzymatic electrochemical glucose sensors based on screen-printed graphite macroelectrodes modified via a facile methodology with Ni, Cu, and Ni/Cu hydroxides are shown to accurately determine glucose in real human serum blood samples, Anal. Methods 25 (2021) 2812–2822.
[52] M.L. Chelaghmia, M. Nacef, A.M. Affoune, M. Ponti´e, T. Derabla, Facile Synthesis of $Ni(OH)_2$ Modified Disposable Pencil Graphite Electrode and its Application for Highly Sensitive Non-enzymatic Glucose Sensor, Electroanalysis 30 (2018) 1117–1124.
[53] A. S¸avk, H. Aydın, K. Cellat, F. S¸en, A novel high performance non-enzymatic electrochemical glucose biosensor based on activated carbon-supported Pt–Ni nanocomposite, J. Mol. Liq. 300 (2020) 112355.
[54] N.F.B. Azeredo, P.O. Rossini, J.M. Gonçalves, G.L. Assis, K. Araki, L. Angnes, Nanostructured mixed Ni/Pt hydroxides electrodes for BIA-amperometry determination of hydralazine, J. Taiwan Inst. Chem. Eng. 95 (2019) 475–480.
[55] L. Zhang, H. Li, J. Gu, X. Zhao, X. Wang, Facile one-step synthesis of Pt/$Ni(OH)_2$ nanoflakes as sensitive electrode for detection of ammonia–nitrogen in drinking water, Mater. Lett. 328 (2022) 133090.
[56] M.L. Chelaghmia, M. Nacef, A.M. Affoune, Ethanol electrooxidation on activated graphite supported platinum–nickel in alkaline medium, J. Appl. Electrochem. 42 (2012) 819–826.
[57] M. Khairy, A.A. Khorshed, F.A. Rashwan, G.A. Salah, H.M. Abdel-Wadood, C. E. Banks, Sensitive determination of amlodipine besylate using bare/unmodified and DNA-modified screen-printed electrodes in tablets and biological fluids, Sens. Actuators B Chem. 239 (2017) 768–775.
[58] M. Khairy, H.A. Ayoub, C.E. Banks, Non-enzymatic electrochemical platform for parathion pesticide sensing based on nanometer-sized nickel oxide modified screen-printed electrodes, Food Chem. 255 (2018) 104–111.
[59] N. Herna´ndez-Iba´n˜ez, I. Sanjua´n, M.A´. Montiel, C.W. Foster, C.E. Banks, J. Iniesta, L-Cysteine determination in embryo cell culture media using Co(II)-phthalocyanine modified disposable screen-printed electrodes, J. Electroanal. Chem. 780 (2016) 303–310.
[60] E. Bernalte, M. Carroll, C.E. Banks, New electrochemical approach for the measurement of oxidative DNA damage: voltammetric determination of 8-oxo-guanine at screen-printed graphite electrodes, Sens. Actuators B Chem. 247 (2017) 896–902.
[61] W. Drissi, M.L. Chelaghmia, M. Nacef, A.M. Affoune, H. Satha, R. Kihal, H. Fisli, C. Boukharouba, M. Ponti´e, In situ growth of $Ni(OH)_2$ nanoparticles on 316L stainless steel foam: an efficient three-dimensional non-enzymatic glucose electrochemical sensor in real human blood serum samples, Electroanalysis 34 (2022) 1735–1744.
[62] M.A.A. Rahim, H.B. Hassan, R.M.A. Hameed, Graphite electrodes modified with platinum–nickel nano-particles for methanol oxidation, Fuel Cells 4 (2007) 298–305.
[63] R.S. Nicholson, Theory and application of cyclic voltammetry for measurement of electrode reaction kinetics, Anal. Chem. 37 (1965) 1351–1355.
[64] L.R. Cumba, C.W. Foster, D.A.C. Brownson, J.P. Smith, J. Iniesta, B. Thakur, D. R. do Carmo, C.E. Banks, Can the mechanical activation (polishing) of screen-printed electrodes enhance their electroanalytical response? Analyst 141 (2016) 2791–2799.
[65] P. Shaikshavali, T.M. Reddy, V.N. Palakollu, R. Karpoormath, Y.S. Rao, G. Venkataprasad, T.V. Gopal, P. Gopal, Multi walled carbon nanotubes supported CuO–Au hybrid nanocomposite for the effective application towards the electrochemical determination of acetaminophen and 4-aminophenol, Synth. Met. 252 (2019) 29–39.
[66] R.D. Crapnell, C.E. Banks, Perspective: what constitutes a quality paper in electroanalysis? Talanta 4 (2021) 100065.
[67] Y. Sun, H. Yang, X. Yu, H. Meng, X. Xu, A novel non-enzymatic amperometric glucose sensor based on hollow Pt–Ni alloy nanotubes array electrode with enhanced sensitivity, RSC Adv. 86 (2015) 69899–70702.
[68] Q. Sheng, D. Liu, J. Zheng, A nonenzymatic electrochemical nitrite sensor based on Pt nanoparticles loaded $Ni(OH)_2$/multi-walled carbon nanotubes nanocomposites, J. Electroanal. Chem. 796 (2017) 9–16.
[69] Y.V.M. Reddy, B. Sravani, H. Maseed, T. Łuczak, M. Osin´ska, L. SubramanyamSarma, V.V.S.S. Srikanth, G. Madhavi, Ultrafine Pt–Ni bimetallic nanoparticles anchored on reduced graphene oxide nanocomposites for boosting electrochemical detection of dopamine in biological samples, New J. Chem. 20 (2018) 16387–17140.
[70] J. Ahmed, M.M. Rahman, I.A. Siddiquey, A.M. Asiri, M.A. Hasnat, Efficient hydroquinone sensor based on zinc, strontium and nickel based ternary metal oxide (TMO) composites by differential pulse voltammetry, Sens. Actuators B Chem. 256 (2018) 383–392.
[71] N.F. Atta, A. Galal, D.M. El-Said, A novel electrochemical sensor for paracetamol based on β-cyclodextrin/nafion®/polymer nanocomposite, Int. J. Electrochem. Sci. 10 (2015) 1404–1419.
[72] Y. Song, Y. Zhang, J. Li, C. Tan, Y. Li, Preparation of poly ionic liquid-mesoporous carbon nanospheres and its application in simultaneous determination of hydroquinone and catechol, and detection of paracetamol, J. Electroanal. Chem. 865 (2020) 114157.
[73] Q. Guan, H. Guo, N. Wu, Y. Cao, M. Wang, L. Zhang, W. Yang, Highly sensitive determination of acetaminophen and 4-aminophenol based on COF/3D NCNF-T/Au NPs composite electrochemical sensing platform, Colloids Surf. A Physicochem. Eng. Asp. 630 (2021) 127624.
[74] E. laviron, General expression of the linear potential sweep voltammogram in the case of diffusionless electrochemical systems, J. Electroanal. Chem. 101 (1979) 19–28.
[75] S. Abdi, M.L. Chelaghmia, R. Kihal, C.E. Banks, A.G.M. Ferrari, H. Fisli, M. Nacef, A.M. Affoune, M.E.H. Benhamza, Simultaneous determination of 4-aminophenol and paracetamol based on CS–Ni nanocomposite-modified screen-printed disposable electrodes, Monatsh, Chemie 154 (2023) 563–575.
[76] H. Guo, T. Fan, W. Yao, W. Yang, N. Wu, H. Liu, M. Wang, W. Yang, Simultaneous determination of 4-aminophenol and acetaminophen based on high electrochemical performance of ZIF–67/MWCNT–COOH/Nafion composite, Microchem. J. 158 (2020) 105262.
[77] N. Ruecha, N. Rodthongkum, D.M. Cate, J. Volckens, O. Chailapakul, C.S. Henry, Sensitive electrochemical sensor using a graphene-polyaniline nanocomposite for simultaneous detection of Zn(II), Cd(II), and Pb(II), Anal. Chim. Acta 874 (2015) 40–48.
[78] U. Injang, P. Noyrod, W. Siangproh, W. Dungchai, S. Motomizu, O. Chailapakul, Determination of trace heavy metals in herbs by sequential injection analysis-anodic stripping voltammetry using screen-printed carbon nanotubes electrodes, Anal. Chim. Acta 668 (2010) 54–60.
[79] N.M. Thanh, N.V. Hop, N.D. Luyen, N.H. Phong, T.T.T. Toan, Simultaneous determination of Zn(II), Cd(II), Pb(II), and Cu(II) using differential pulse anodic stripping voltammetry at a bismuth film-modified electrode, Adv. Mater. Sci. Eng. 11 (2019) 1826148.
[80] J. Du, R. Yue, F. Ren, Z. Yao, F. Jiang, P. Yang, Y. Du, Novel graphene flowers modified carbon fibers for simultaneous determination of ascorbic acid, dopamine and uric acid, Biosens. Bioelectron. 53 (2014) 220–224.
[81] R. Sha, S. Badhulika, Facile green synthesis of reduced graphene oxide/tin oxide composite for highly selective and ultra-sensitive detection of ascorbic acid, J. Electroanal. Chem. 816 (2018) 30–37.
[82] H. Yang, J. Zhao, M. Qiu, P. Sun, D. Han, L. Niu, G. Cui, Hierarchical bi-continuous Pt decorated nanoporous Au–Sn alloy on carbon fiber paper for ascorbic acid, dopamine and uric acid simultaneous sensing, Biosens. Bioelectron. 124–125 (2019) 191–198.
[83] Y.L. Xie, J. Yuan, H.L. Ye, P. Song, S.Q. Hu, Facile ultrasonic synthesis of graphene/SnO_2 nanocomposite and its application to the simultaneous electrochemical determination of dopamine, ascorbic acid, and uric acid, J. Electroanal. Chem. 749 (2015) 26–30.
[84] R. Zhao, Y. Wang, Z. Zhang, Y. Hasebe, D. Tao, A glassy carbon electrode modified with molybdenite and Ag nanoparticle composite for selectively sensing of ascorbic acid, Anal. Sci. 35 (2019) 733–738.
[85] P.V. Narayana, T.M. Reddy, P. Gopal, G.R. Naidu, Electrochemical sensing of paracetamol and its simultaneous resolution in the presence of dopamine and folic acid at a multi-walled carbon nanotubes/poly(glycine) composite modified electrode, Anal. Methods 6 (2014) 9459–9468.
[86] I. Noviandri, R. Rakhmana, Carbon paste electrode modified with carbon nanotubes and poly(3–aminophenol) for voltammetric determination of paracetamol, Int. J. Electrochem. Sci. 7 (2012) 4479–4487.
[87] G.V. Prasad, V. Vinothkumar, S.J. Jang, D.E. Oh, T.H. Kim, Multi-walled carbon nanotube/graphene oxide/poly(threonine) composite electrode for boosting electrochemical detection of paracetamol in biological samples, Microchem. J. 184 (2023) 108205.
[88] M.P.N. Bui, C.A. Li, K.N. Han, X.H. Pham, G.H. Seong, Determination of acetaminophen by electrochemical co-deposition of glutamic acid and gold nanoparticles, Sens. Actuators B Chem. 174 (2012) 318–324.
[89] N. Masihpour, S.K. Hassaninejad-Darzi, A. Sarvary, Nickel–cobalt salen organometallic complexes encapsulated in mesoporous NaA nanozeolite for electrocatalytic quantification of ascorbic acid and paracetamol, J. Inorg. Organomet. Polym Mater. 33 (2023) 2661–2680.